ACS APPLIED MATERIALS & INTERFACES

Research Article

www.acsami.org

SGO/SPES-Based Highly Conducting Polymer Electrolyte Membranes for Fuel Cell Application

Swati Gahlot,[†] Prem Prakash Sharma,[†] Vaibhav Kulshrestha,*[,†,‡] and Prafulla K Jha[§]

[†]CSIR-Central Salt and Marine Chemicals Research Institute (CSIR-CSMCRI), and [‡]Academy of Scientific and Innovative Research, CSIR-Central Salt and Marine Chemicals Research Institute (CSIR-CSMCRI), Council of Scientific & Industrial Research (CSIR), Gijubhai Badheka Marg, Bhavnagar 364 002, Gujarat, India

[§]Department of Physics, The M S University of Baroda, Vadodara, Gujarat, India

Supporting Information

ABSTRACT: Proton-exchange membranes (PEMs) consisting of sulfonated poly(ether sulfone) (SPES) with enhanced electrochemical properties have been successfully prepared by incorporating different amount of sulfonated graphene oxide (SGO). Composite membranes are tested for proton conductivity (30−90 °C) and methanol crossover resistance to expose their potential for direct methanol fuel cell (DMFC) application. Incorporation of SGO considerably increases the ion-exchange capacity (IEC), water retention and proton conductivity and reduces the methanol permeability. Membranes have been characterized by FTIR, XRD, DSC, SEM, TEM, and AFM techniques. Intermolecular interactions between the components in composite membranes are established by FTIR. The distribution of SGO throughout the membrane matrix has been examined using SEM and TEM and found to be uniform. The maximum proton conductivity has been found in 5% SGO composite with higher methanol crossover resistance.

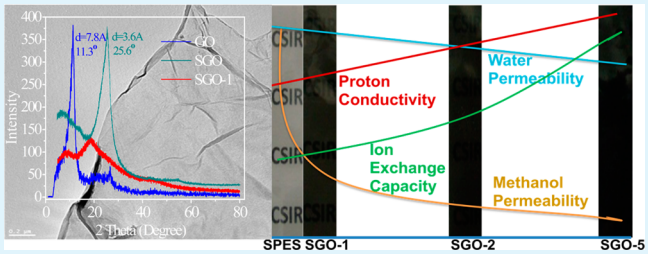

KEYWORDS: *poly(ether sulfone), graphene oxide, PEMs, proton conductivity, thermomechanical properties*

INTRODUCTION

Polymer electrolyte membranes (PEMs) are being studied extensively because of their use in energy conversion devices and high temperature applications.[1,2] Commercially available membrane used in PEMFCs is Nafion because of its excellent chemical stability and high conductivity. However, high cost and methanol crossover still hinders its application in PEMFCs.[3,4] Thus, the development of inexpensive proton exchange membranes having better performance and comparative properties for fuel cell application is the area of research to explore. Emphasis is being given to fabricate the membranes with high proton conductivity and low cost.[5−9]

SPES is a thermomechanically stable polymer widely used in PEMs application that contains sulfonic acid groups in its backbone. At higher degree of sulfonation of PES, swelling is the major drawback, which limits their use as PEMs. Therefore, the properties of the SPES membranes have to be improved, which could be accomplished by blending them with fillers. Incorporation of organic/inorganic materials can greatly improve the applicability of SPES as PEMs.[10,11] However, limited studies are available showing that the incorporation of organic/inorganic materials into SPES membranes for DMFC application.[12,13] In days, remarkable properties of graphene oxide have attracted tremendous attention in wide range of areas.[14−18] The excellent structural, mechanical and thermal properties of Graphene offer large possibilities to be tailored in different applications. For the realization of graphene in different applications it is essential to tune up its chemical and electronic structure to fulfill the specific requirements.[19,20] Graphene can be easily functionalized to convert into graphene oxide (GO) with improved properties. Large surface area and electronic insulation provide GO a platform to be used as organic filler in PEMs. The oxygen containing groups e.g. epoxy, hydroxyl etc. enables GO for further modification by chemical reactions and for introduction of various functional groups onto its sheets. Substituting hydroxyl/epoxy groups of GO with $-HSO_3$ group enhances its activity.[21] Nanocomposties based on SGO and SPES can have improved proton conductivity, Ion exchange capacity as well as mechanical strength because of the strong interaction between the large surface area of SGO and the SPES. The objective of the present study to prepare the low cost highly conducting PEM that can be used for the DMFC and high temperature applications.

Present manuscript describes the development of SGO/SPES based nanocomposite membranes with various SGO concentrations (0.5, 1, 2, and 5%) and named as SGO-05 (0.5%), SGO-1 (1%), SGO-2(2%), and SGO-5 (5%). Chemical, structural, thermal and mechanical characterizations are done using respective analysis techniques. Membranes were

Received: January 7, 2014
Accepted: April 3, 2014
Published: April 3, 2014

   dx.doi.org/10.1021/am5000504 | ACS Appl. Mater. Interfaces 2014, 6, 5595−5601

studied extensively by electrochemical and physiochemical properties. Proton conductivity at different temperatures is measured to evaluate membranes performance at high temperature. Membrane shows the low methanol permeability and low activation energy for the proton conduction.

EXPERIMENTAL SECTION

Materials and Methods. Poly(ether sulfone) Gafone-3300, obtained from Gharda Chemicals Pvt Ltd., India, is used after drying under vacuum for 24 h. Graphite powder was purchased from Sigma-Aldrich. Other chemicals are obtained commercially and used as received without further purification.

GO was synthesized by the modified Hummers method using graphite powder as the starting material.[22] SGO is achieved by the functionalization of GO by concentrated sulfuric acid followed by chlorosulfonic acid. In a typical method, 250 mg of GO is treated with 75 mL of sulfuric acid first for 1 h and then 15 mL of chlorosulfonic acid is added dropwise to this solution. The mixrure is stirred for 24h under nitrogen atmosphere at room temperature. After the completion of reaction the solution is added to diethyl ether dropwise at 0−5 °C with stirring. Afterward, the obtained mixture is centrifuged to separate the precipitates. To remove impurities solid product is repeatedly washed with diethyl ether to recover SGO. Sulfonation of PES was carried out as reported earlier using conc. H_2SO_4 (95−98%) under vigorous stirring at 60 °C for 6 h.[23] The SGO/SPES composite membranes are obtained from a highly homogeneous solution of SPES and SGOs under sonication in DMAC, followed by solution casting on a glass plate with the help of doctors blade. The membranes are dried at 100 °C in vacuum oven for 24 h to complete removal of solvent. Membranes with different SGO concentration (0, 0.5, 1, 2, and 5 wt %) were prepared and designated as SPES, SGO-05, SGO-1, SGO-2, and SGO-5, respectively.

Chemical and Structural Characterization. The samples have been characterized by the means of chemical and structural properties, details of the characterization are included in the Supporting Information.

Stability of Membranes. Thermo-mechanical stabilities of the membrane samples are evaluated by the DMA, TGA, and DSC. Details of the characterization are included in Supporting Information.

Physiochemical Characterization. Water Uptake behavior of membranes is determined by recording the weight gain after equilibrating in water for 24h. Ion exchange capacity (IEC) of composite membranes was estimated by the acid base titration. Proton conductivity of the membranes was measured on potentiostat/galvanostat (Auto Lab, Model PGSTAT 30). Details of the experiments are given in the Supporting Information.

Methanol Permeability. Methanol Permeability of the membranes is carried out in a two compartment cell in recirculation mode at room temperature. Membranes are equilibrated in feed solution for 4 h before performing the experiments. The initial and final concentration of the solution is measured by using a digital refractometer (Mettler tolado refratometer). Methanol Permeability was finally obtained by the following equation[24]

$$P = \frac{1}{A}\frac{C_B(t)}{C_A(t - t_0)}V_B l$$

where A is the effective membrane area, l is the membrane thickness, $C_B(t)$ is methanol concentration in compartment B at time t, while $C_A(t)$ is the change in concentration of methanol initially to time t in compartment A. V_B is the volume of compartment B. For the suitability of membrane for fuel cell, we calculate the selectivity of the membrane by following equation

$$S_P = \frac{\sigma}{P_M}$$

where P_M is the methanol permeability (cm^2/s), and σ is the membrane conductivity (S cm^{-1}).

RESULTS AND DISCUSSION

Structural Characterization of GO, SGO, and Composite Membranes. FTIR spectra of GO and SGO has been shown in Figure 1. The difference between two can be

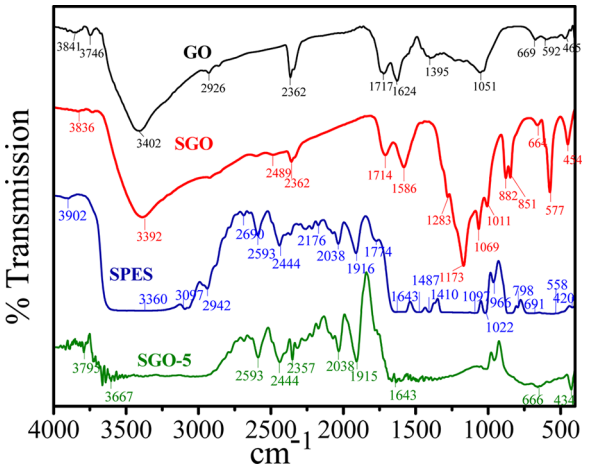

Figure 1. FTIR spectra of GO, SGO, SPES, and SGO-5 Membrane.

demonstrated by the addition of a new functional groups on GO at 1283 and 1173 cm^{-1} which attributes the absorption of sulfonic acid group ($-SO_3H$).[25,26] The stretching frequency at 3360 cm^{-1} in SPES and 3667 cm^{-1} in SGO-5 indicate O−H vibration (hydrogen bond) whereas for SPES, the frequencies at 2942, 2785, 2690, and 2593 cm^{-1} for SPES & SGO-5 indicate the presence of O−H stretching (acidic group). The vibration band at 2176 cm^{-1} for SPES is due to the presence of C═C stretching. It can be seen that there is a peak shift in SGO-5 compared to SPES membrane, which shows the interaction of SGO to the SPES matrix. XRD patterns of GO and SGO are displayed in Figure 2. It can be seen from the

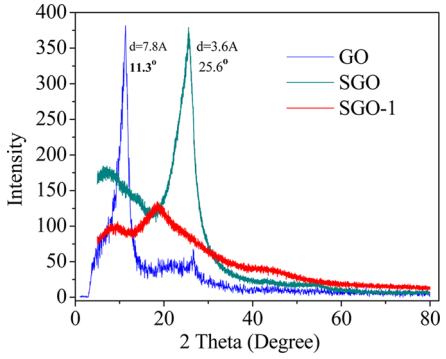

Figure 2. XRD patterns for GO, SGO, and SGO composite membrane.

figure that GO has the diffraction angle (2θ) and interplanar spacing values as 11.3° and 7.8 Å, respectively, whereas SGO peak is observed at 25.6° and at 3.6 Å, the reduction in interplanar spacing is caused by the partial restacking through $\pi-\pi$ interaction and the removal of oxygen functional groups after sulfonation.[27] The shifting of peak toward the higher 2θ is due to the addition of sulfonic acid group in SGO as reported in literature.[25] The interaction between SGO and SPES can be seen in diffraction peak at 18.5° for SGO-1 membrane.

dx.doi.org/10.1021/am5000504 | ACS Appl. Mater. Interfaces 2014, 6, 5595−5601

The morphological features of SGO can be seen in SEM micrograph at different magnification (Figure 3A) that shows

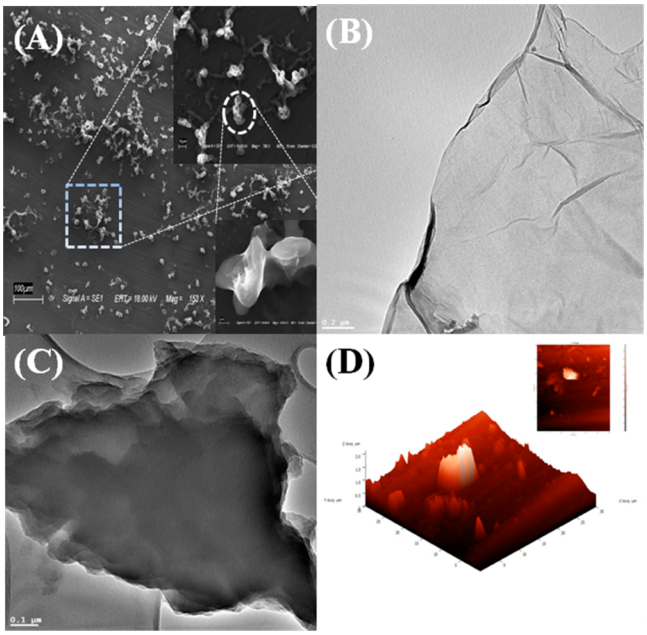

Figure 3. (A) SEM of SGO, (B, C) TEM of SGO, and (D) 2D and 3D AFM of SGO.

the formation of chain like structure in SGO. The squared area shows magnified SGO image in the upper inset, whereas the circled area shows the highly magnified image of SGO (lower inset) at 2 μm. Images A and B in Figure 3 show the sheetlike structures of GO and SGO, respectively. The wrinkled structure of GO shows consistent results compared with the literature,[28,29] SGO image looks much darker in color as compared to GO. The average size of the GO and SGO sheets are found to be 4 μm^2. Figure 3D shows the two and three-dimensional image of SGO particle taken by AFM. Figure 4

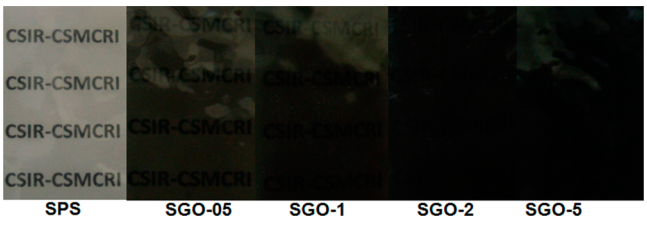

Figure 4. Photograph of different composite membranes.

shows the digital photograph of SPES and composite membranes; it is clear from the figure that increasing the SGO content in SPES reduced the transparency of the membranes and membranes get darker in color. The structure of composite membranes analyzed by the AFM, SEM and TEM are display in Figure 5. Cross-sectional views of SGO-05 and SGO-1 show the distribution of SGO in SPES (Figure 5E, F). It is clear from the figure that the distribution of SGO in the SPES matrix is uniform, which is confirmed by the TEM image as shown is Figure 5G. Figure 5A–D shows the AFM images of SPES, SGO-05, SGO-2, and SGO-5 and is used to determine the surface roughness of the membranes. The surface roughness calculated by images is found to be in increasing order by increasing the amount of SGO and reached up to 12.05 nm from 4.87 nm to its initial value (SPES).

Thermomechanical Stability of Composite Membrane. Prepared GO, SGO, and composite membranes are analyzed thermally by the means of TGA and DSC, and mechanical analysis are performed by DMA. Figures S-1 and S-2 in the Supporting Information displays the weight loss and their derivative for GO and SGO. GO and SGO both show the similar trend throughout the temperature range from 30 to 600 °C. The weight loss of GO is 53%, whereas 56.4% weight is observed for SGO up to 600 °C. GO and SGO both reveal weight loss below 100 °C, which is attributed to the absorbed water and at 150 °C weight loss is caused by bounded water. Loss of oxygen=containing functionalities such as CO and CO_2 is the reason for second weight loss between 150 and 220 °C for both GO and SGO. The third weight loss of SGO at 258 °C is due to the decomposition of sulfonic acid group. Twenty-five percent weight loss from 220 to 400 °C is due to the weakening of van der Waals forces between the GO layers.[25] Composite membranes are also analyzed by TGA. Three step weight losses are observed between the range 50−100, 250−350, and above 500 °C (Figure 6). All three weight losses are similar for SPES membrane, but the composite membranes show delayed weight loss. The first weight loss is due to the loss of bound water, the second weight loss is associated with the dissociation of sulfonic acid group present in the membranes, and the final weight loss above 500 °C is assigned to decomposition of polymer backbone present in SPES.[30] Results confirm the interaction between SPES and SGO. DSC thermograms for prepared membranes are shown in Figure S-3 in the Supporting Information. The figure shows that the crystallization peak of SPES appears at about 65.9 °C, whereas for SGO-5, it goes to 152 °C because of the interaction between SGO and SPES. DSC results support the TGA and shows that SGO-5 membrane is highly stable than the other membranes. Figure 7 shows that the modulus values of composite membranes increases by SGO content. The modulus value for SGO-5 increased by 27% compared to the SPES. The temperature of tan δ also increases by increasing SGO content and confirm the higher thermomechanical stability of composite membranes computed by DMA analysis (see Figure S-4 in the Supporting Information).[31,32]

Water Retention Capability, Water Uptake Behavior and Ion Exchange Capacity. Kinetics of water uptake and retention play an important role in PEMs for fuel cell application. The membrane's water uptake is measured gravimetrically by equilibrating the membranes in water. The (H_2O/SO_3H) water content/hydration number, λ is calculated using the following equation

$$\lambda = \left(\frac{W_{wet} - W_{dry}}{18.01}\right)\left(\frac{1000}{W_{dry}IEC}\right)$$

The λ value for SPES is calculated about 4.8, which goes to increases by 5.93 for SGO-5 membrane. The increment in λ is due to the corresponding ion exchange capacity of the PES, the IEC for SGO-5 is found to be 16.5% higher than SPES membrane because of the presence of highly acidic functionalized SGO as shown is Table 1. It is clear from the results that by increasing the SGO content the water molecules surround to SO_3H increases from 4.8 to 5.93. Unfortunately the higher water uptake reduces the mechanical properties but in this case there is no reduction found due to the interaction of SGO with

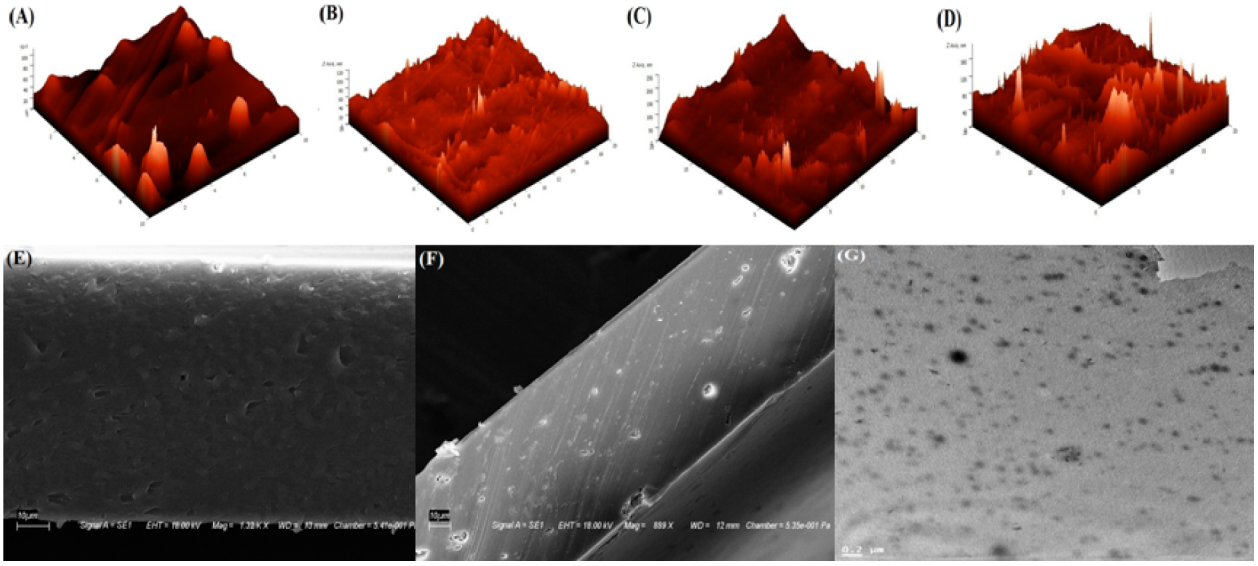

Figure 5. (A–D) AFM of SPES, SGO-05, SGO-2, SGO-5, and (E, F) SEM of SGO-05, SGO-1; (G) TEM of SPES/SGO composite.

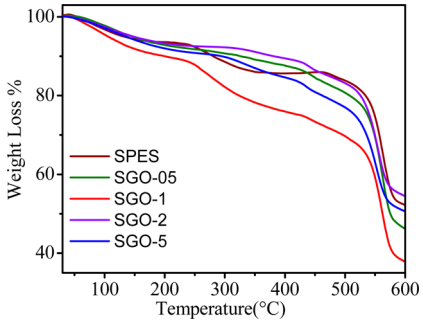

Figure 6. TGA thermograph for different SPES/SGO composite membranes.

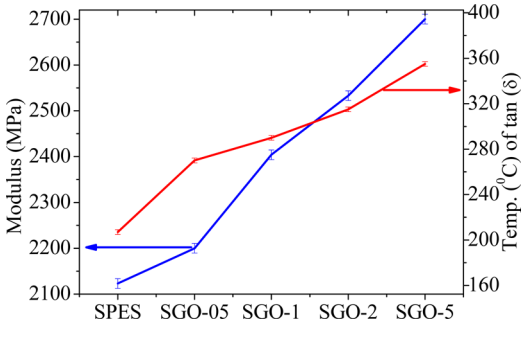

Figure 7. Storage modulus and temperature (tan δ) for different SPES/SGO composite membranes (maximum error for modulus is ±0.1% and for tan δ is ±0.5%).

SPES matrix.[23,30] Two types of water are available in PEMs, bound water and the free water. Bound water is found to be more responsible for the proton conduction. The amount of bound water is calculated by TGA analysis from 100 to 150 °C,[33] whereas the free water is the difference of total water to the bound water. SPES membranes shows the lowest bound water content (2.58%) in comparison with all membranes, whereas there is 3.07% bound water in SGO-5 composite membrane; more bound water in SGO-5 gives it higher water retention availability and greater proton conduction.

Proton Conductivity and Diffusion Coefficient Measurements. For high-temperature applications, membrane proton conductivity is measured for each membrane from 30 to 90 °C and the corresponding values are depicted in Figure 8

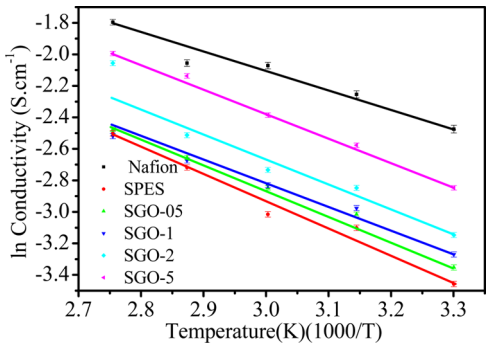

Figure 8. Arrhenius plot of conductivity vs temperature for different membranes (maximum error for conductivity is ±0.5%).

Table 1. Ion Exchange Capacity, Number of Water Molecules Per Ionic Site (λ), Water Uptake (%), Free and Bound Water % for Different PEMs

membrane type	IEC (mequiv g^{-1})	λ (SO_3/H_2O)	water uptake %	free water %	bound water %
SPES	1.40 ± 0.05	4.80 ± 0.1	12.12 ± 0.5	9.54 ± 0.5	2.58 ± 0.5
SGO-05	1.45 ± 0.05	5.21 ± 0.1	13.62 ± 0.5	10.55 ± 0.5	3.07 ± 0.5
SGO-1	1.48 ± 0.05	5.59 ± 0.1	14.90 ± 0.5	11.10 ± 0.5	3.80 ± 0.5
SGO-2	1.56 ± 0.05	5.77 ± 0.1	16.23 ± 0.5	13.60 ± 0.5	2.63 ± 0.5
SGO-5	1.63 ± 0.05	5.93 ± 0.1	17.41 ± 0.5	14.34 ± 0.5	3.07 ± 0.5

dx.doi.org/10.1021/am5000504 | ACS Appl. Mater. Interfaces 2014, 6, 5595–5601

Table 2. Membrane Conductivity (σ), Diffusion Coefficient (D_σ), Methanol Permeability (P_m), Selectivity (S), and Activation Energy of Proton Conduction (E_a) of Different PEMs

membrane type	σ ($\times 10^{-2}$ S cm^{-1})	D_σ ($\times 10^{-10}$ m^{2}S^{-1})	P_m ($\times 10^{-7}$ cm^{2}S^{-1})	S ($\times 10^5$)	E_a (kJ mol^{-1})
SPES	3.15 ± 0.01	1.845 ± 0.05	1.827 ± 0.1	1.72414 ± 0.1	21.01 ± 0.5
SGO-05	3.50 ± 0.01	2.082 ± 0.05	1.611 ± 0.1	2.17256 ± 0.1	17.50 ± 0.5
SGO-1	3.80 ± 0.01	2.205 ± 0.05	1.598 ± 0.1	2.37797 ± 0.1	15.92 ± 0.5
SGO-2	4.30 ± 0.01	2.741 ± 0.05	1.582 ± 0.1	2.71808 ± 0.1	14.32 ± 0.5
SGO-5	5.8 ± 0.01	3.432 ± 0.05	1.556 ± 0.1	3.72751 ± 0.1	12.36 ± 0.5

and Table 2. Proton conductivities of the membranes are calculated from the Nyquist plots with different SGO content from 0.5 to 5 and are presented in Table 2. The proton conductivity increases with SGO content in membranes because of enhanced proton mobility resulting from the increased λ value.[34−37] The proton conductivity of the SPES membrane is calculated to 3.15×10^{-2} S cm^{-1} at 30 °C, which is raised up to 5.8×10^{-2} S cm^{-1} for the SGO-5 membrane. The 86% increment in conductivity is due to the higher IEC, higher water retention capacity, higher λ value, and the higher number of available sulfonic group sites in the membrane. High IEC provides adequate acidic groups inside the membrane and a high water uptake makes the proton diffusion easy.[38,39] Acidic functional groups ($-SO_3H$) of polyelectrolyte membranes dissociate because of hydration and allow transport of hydrated proton $(H_3O)^+$. Temperature also plays an important role in proton conductivity. Conductivity of all the membranes found to be increased by 2.5 times on increasing the temperature from 30 to 90 °C that may be due to the increment in proton diffusion with temperature.[40] In the case of the SGO-5 membrane, the conductivity is comparable with the Nafion-117 membrane for the whole temperature range.

Activation energy for proton conduction reveals the minimum energy required for proton transport from a functional group to another and is, therefore, an important parameter of a PEM. Temperature-dependent proton conductivity is used to determine the activation energy for proton conduction. The Arrhenius-type plot shown in Figure 8 is used to calculate the activation energy for PEMs.[40] Table 2 shows that the activation energy of the SPES membrane has a higher value than that for Nafion-117. By increasing the SGO content in SPES, the required activation energy reduced as shown in Table 2. The dependence of proton diffusion coefficient on SGO content is evaluated by the Nernst−Einstein equation using membrane conductivity.[41] Calculated values of D^σ for different membranes are also presented in Table 2, shows that the D^σ value increases by increasing the SGO content in SPES matrix. This indicates that the incorporation of SGO can increase the applicability of the SPES membranes in DMFC.

Methanol Permeation (P_M) Resistance and Selectivity of Hybrid Membranes. High methanol permeation resistance with high proton conductivity is the basic requirement for the PEM's for DMFC application. Methanol permeability of SPES and SGO/SPES membranes is shown in Table 2. It can be seen that the methanol permeability of SGO/SPES membranes decreased with increasing SGO content. In the case of the SGO/SPES membrane, SGO prevents the movement of methanol through the membrane and act as a barrier for connected hydrophilic channels as well as provides the higher conductivity to the composite membrane. The interaction between SGO and SPES restricts the formation of the channels in membranes, which leads to low methanol permeability. Methanol permeability for the SPES membrane is found to be 1.827×10^{-7} cm^2 S^{-1}, which reduces to 1.611×10^{-7} cm^2 S^{-1} for SGO-05 and 1.582×10^{-7} cm^2 S^{-1} for SGO-2 membranes and finally reached to 1.556×10^{-7} cm^2 S^{-1} for SGO-5 membrane. Reduction in methanol permeability for SGO/SPES membrane is due to strong interfacial adhesion between SGO particle and SPES matrix.[42] For the suitability of the membrane for fuel cell, we calculate the selectivity of the membrane, which is directly proportional to the membrane conductivity and inversely proportional to the methanol permeability. The selectivity of the SPES membrane is found to be 1.724×10^5, which increases in composite membranes and reaches 3.727×10^5 for SGO-5 membrane (Table 2). The low methanol permeability and high selectivity of SGO-5 membrane make it suitable for the DMFC application.

CONCLUSION

Incorporation of small amounts of SGO in SPES is confirmed to be a novel scheme to enhance the properties of proton-exchange SPES membranes. While IEC, conductivity, methanol permeation resistance and selectivity of the membranes are enhanced, the membrane still maintained excellent thermo-mechanical stability. Prepared membranes show good proton conductivity at temperatures ranging from 30 to 90 °C and have reduced activation energy for proton conduction by SGO addition. Figure 9 summarizes the influence of SGO on different membrane properties relevant for electrochemical application. The good comprehensive performance and dimension stability make the SPES/SGO hybrid membranes an ideal candidate for fuel cells and other high-temperature applications.

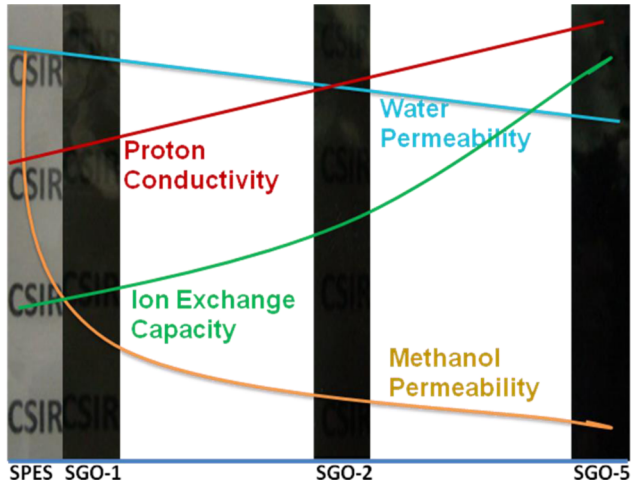

Figure 9. Different membrane properties by inclusion of sulfonated graphene oxide content.

dx.doi.org/10.1021/am5000504 | ACS Appl. Mater. Interfaces 2014, 6, 5595−5601

■ ASSOCIATED CONTENT

Supporting Information

Detail of the chemical, structural, physiochemical characterization, and membrane stability are included as section S1−S3, as well as Figures S-1−S-4. This material is available free of charge via the Internet at http://pubs.acs.org/.

■ AUTHOR INFORMATION

Corresponding Author

*E-mail: vaibhavk@csmcri.org or vaibhavphy@gmail.com. Tel.: +91-278-2567039. Fax: +91-278-2567562.

Notes

The authors declare no competing financial interest.

■ ACKNOWLEDGMENTS

Author V.K. is thankful to the Department of Science and Technology, New Delhi, for providing fund under the WTI scheme. The authors are also thankful to Analytical Discipline and Centralized Instrument facility, CSMCRI, Bhavnagar, for instrumental support.

■ REFERENCES

(1) Kannan, R.; Kakade, B. A.; Pillai, V. K. Polymer Electrolyte Fuel Cells Using Nafion-Based Composite Membranes with Functionalized Carbon Nanotubes. *Angew. Chem., Int. Ed.* **2008**, *47*, 2653−2656.

(2) Miyatake, K.; Tombe, T.; Chikashige, Y.; Uchida, H.; Watanabe, M. Enhanced Proton Conduction in Polymer Electrolyte Membranes with Acid-Functionalized Polysilsesquioxane. *Angew. Chem., Int. Ed.* **2007**, *46*, 6646−6649.

(3) Lin, H. L.; Wang, S. H. Nafion/ Poly(vinyl alcohol) Nano-fiber Composite and Nafion/ Poly(vinyl alcohol) Blend Membranes for Direct Methanol Fuel Cells. *J. Membr. Sci.* **2014**, *452*, 253−262.

(4) Omosebi, A.; Besser, R. S. Electron Beam Patterned Nafion Membranes for DMFC Applications. *J. Power Sources* **2013**, *228*, 151−158.

(5) Nagarale, R. K.; Shin, W.; Singh, P. K. Progress in Ionic Organic-Inorganic Composite Membranes for Fuel Cell Applications. *Polym. Chem.* **2010**, *1*, 388−408.

(6) Ladewig, B. P.; Knott, R. B.; Hill, A. J.; Riches, J. D.; White, J. W.; Martin, D. J.; Diniz da Costa, J. C.; Lu, G. Q. Physical and Electrochemical Characterization of Nanocomposite Membranes of Nafion and Functionalized Silicon Oxide. *Chem. Mater.* **2007**, *19*, 2372−2381.

(7) Karim, M. R.; Hatakeyama, K.; Matsui, T.; Takehira, H.; Taniguchi, T.; Koinuma, M.; Matsumoto, Y.; Akutagawa, T.; Nakamura, T.; Noro, S.; Yamada, T.; Kitagawa, H.; Hayami, S. Graphene Oxide Nanosheet with High Proton Conductivity. *J. Am. Chem. Soc.* **2013**, *135*, 8097−8100.

(8) Klaysom, C.; Moon, S. H.; Ladewiga, B. P.; Max Lua, G. Q.; Wang, L. Preparation of Porous Ion-Exchange Membranes (IEMs) and Their Characterizations. *J. Membr. Sci.* **2011**, *371*, 37−44.

(9) Antolini, E.; Gonzalez, E. R. Polymer Supports for Low-Temperature Fuel Cell Catalysts. *Appl. Catal., A* **2009**, *365*, 1−19.

(10) Lim, Y.; Lee, S.; Seo, D.; Jang, H.; Hossain, M.; Ju, H.; Hong, T.; Kim, W. Sulfonated Poly(ethersulfone) Electrolytes Structured with Mesonaphthobifluorene Graphene Moiety for PEMFC. *Int. J. Hydrogen Energy* **2014**, *39*, 1532−1538.

(11) Sgreccia, E.; Di Vona, M. L.; Knauth, P. Hybrid Composite Membranes Based on SPEEK and Functionalized PPSU for PEM Fuel Cells. *Int. J. Hydrogen Energy* **2011**, *36*, 8063−8069.

(12) Tripathi, B. P.; Shahi, V. K. Organic−Inorganic Nanocomposite Polymer Electrolyte Membranes for Fuel Cell Applications. *Prog. Polym. Sci.* **2011**, *36*, 945−979.

(13) Wen, S.; Gong, C.; Tsen, W. C.; Shu, Y. C.; Tsai, F. C. Sulfonated Poly(ethersulfone) (SPES)/Boronphosphate (BPO_4) Composite Membranes for High-Temperature Proton-Exchange Membrane Fuel Cells. *Int. J. Hydrogen Energy* **2009**, *34*, 8982−8991.

(14) Novoselov, K. S.; Geim, A. K.; Morozov, S. V.; Jiang, D.; Zhang, Y.; Dubonos, S. V.; Grigorieva, I. V.; Firsov, A. A. Electric Field Effect in Atomically Thin Carbon Films. *Science* **2004**, *306*, 666−669.

(15) Yu, D.; Negelli, E.; Naik, R.; Dai, L. Asymmetrically Functionalized Graphene for Photodependent Diode Rectifying Behavior. *Angew. Chem., Int. Ed.* **2011**, *50*, 6575−6578.

(16) Yu, D.; Yang, Y.; Durstock, M.; Baek, J. B.; Dai, L. Soluble P3HT Grafted Graphene for Efficient Bilayer Heterojunction Photovoltaic Devices. *ACS Nano* **2010**, *4*, 5633−5640.

(17) Qu, L.; Liu, Y.; Baek, J. B.; Dai, L. Nitrogen-Doped Graphene as Efficient Metal-Free Electrocatalyst for Oxygen Reduction in Fuel Cells. *ACS Nano* **2010**, *4*, 1321−1326.

(18) Xie, X.; Qu, L.; Zhou, C.; Li, Y.; Zhu, J.; Bai, H.; Shi, G.; Dai, L. An Asymmetrically Surface-Modified Graphene Film Electrochemical Actuator. *ACS Nano* **2010**, *4*, 6050−6054.

(19) Xue, Y.; Chen, H.; Yu, D.; Wang, S.; Yardeni, M.; Dai, Q.; Liu, Y.; Qu, J.; Dai, L. Oxidizing Metal Ions with Graphene Oxide: The in-situ Formation of Magnetic Nanoparticles on Self-Reduced Graphene Sheets for Multifunctional Applications. *Chem. Commun.* **2011**, *47*, 11689−11691.

(20) Dikin, D. A.; Stankovich, S.; Zimney, E. J.; Piner, R. D.; Dommett, G. H. B.; Evmenenko, G.; Nguyen, S. T.; Ruoff, R. S. Preparation and Characterization of Graphene Oxide Paper. *Nature* **2007**, *448*, 457−460.

(21) Dreyer, D. R.; Park, S.; Bielawski, C. W.; Ruoff, R. S. The Chemistry of Graphene Oxide. *Chem. Soc. Rev.* **2010**, *39*, 228−240.

(22) Chabot, V.; Higgins, D.; Yu, A.; Xiao, X.; Chen, Z.; Zhang, J. A Review of Graphene and Graphene Oxide Sponge: Material Synthesis and Applications to Energy and the Environment. *Energy Environ. Sci.* **2014**, DOI: 10.1039/C3EE43385D.

(23) Thakur, A. K.; Gahlot, S.; Kulshrestha, V.; Shahi, V. K. Highly Stable Acid−Base Complex Membrane for Ethanol Dehydration by Pervaporation Separation. *RSC Adv.* **2013**, *3*, 22014−22022.

(24) Pandey, R. P.; Shahi, V. K. Aliphatic-Aromatic Sulphonated Polyimide and Acid Functionalized Polysilsesquioxane Composite Membranes for Fuel Cell Applications. *J. Mater. Chem. A* **2013**, *1*, 14375−14383.

(25) Kumar, R.; Scott, K. Freestanding Sulfonated Graphene Oxide Paper: A New Polymer Electrolyte for Polymer Electrolyte Fuel Cells. *Chem. Commun.* **2012**, *48*, 5584−5586.

(26) Chen, D.; Feng, H.; Li, J. Graphene Oxide: Preparation, Functionalization, and Electrochemical Applications. *Chem. Rev.* **2012**, *112*, 6027−6053.

(27) Liu, J.; Xue, Y.; Dai, L. Sulfated Graphene Oxide as a Hole-Extraction Layer in High- Performance Polymer Solar Cells. *J. Phys. Chem. Lett.* **2012**, *3*, 1928−1933.

(28) Tang, H.; Ehlert, G. J.; Lin, Y.; Sodano, H. A. Highly Efficient Synthesis of Graphene Nanocomposites. *Nano Lett.* **2012**, *12*, 84−90.

(29) Wilson, N. R.; Pandey, P. A.; Beanland, R.; Young, R.; Kinloch, I.; Gong, L.; Liu, Z.; Suenaga, K.; Rourke, J.; York, S. Graphene Oxide: Structural Analysis and Application as a Highly Transparent Support for Electron Microscopy. *ACS Nano* **2009**, *3*, 2547−2556.

(30) Chakrabarty, T.; Rajesh, A. M.; Jasti, A.; Thakur, A. K.; Singh, A. K.; Prakash, S.; Kulshrestha, V.; Shahi, V. K. Stable Ion-Exchange Membranes for Water Desalination by Electrodialysis. *Desalination* **2011**, *282*, 2−8.

(31) Kulshrestha, V.; Agarwal, G.; Awasthi, K.; Tripathi, B.; Acharya, N. K.; Vyas, D.; Saraswat, V. K.; Vijay, Y. K.; Jain, I. P. Microstructure Change in Poly(ethersulfone) Films by Swift Heavy Ions. *Micron* **2010**, *41*, 390−394.

(32) Kulshrestha, V. Formation of Nano Tracks in PES Films Characterized by Hydrogen Transport and Mechanical Properties. *Int. J. Hydrogen Energy* **2009**, *34*, 9274−9278.

(33) Zhu, X.; Zhang, H.; Zhang, Y.; Liang, Y.; Wang, X.; Yi, B. An Ultrathin Self-Humidifying Membrane for PEM Fuel Cell Application: Fabrication, Characterization, and Experimental Analysis. *J. Phys. Chem. B* **2006**, *110*, 14240−14248.

(34) Zarrin, H.; Higgins, D.; Jun, Y.; Chen, Z.; Fowler, M. Functionalized Graphene Oxide Nanocomposite Membrane for Low Humidity and High Temperature Proton Exchange Membrane Fuel Cells. *J. Phys. Chem. C* **2011**, *115*, 20774−20781.
(35) Heo, Y.; Im, H.; Kim, J. The Effect of Sulfonated Graphene Oxide on Sulfonated Poly (Ether Ether Ketone) Membrane for Direct Methanol Fuel Cells. *J. Membr. Sci.* **2013**, *426*, 11−22.
(36) Lin, C. W.; Lu, Y. S. Highly Ordered Graphene Oxide Paper Laminated with a Nafion Membrane for Direct Methanol Fuel Cells. *J. Power Sources* **2013**, *237*, 187−194.
(37) Choi, B. G.; Hong, J.; Park, Y. C.; Jung, D. H.; Hong, W. H.; Hammond, P. T.; Park, H. S. Innovative Polymer Nanocomposite Electrolytes: Nanoscale Manipulation of Ion Channels by Functionalized Graphenes. *ACS Nano* **2011**, *5*, 5167−5174.
(38) Petrowsky, M.; Frech, R. Application of the Compensated Arrhenius Formalism to Self-Diffusion: Implications for Ionic Conductivity and Dielectric Relaxation. *J. Phys. Chem. B* **2010**, *114*, 8600−8605.
(39) Filipoi, C.; Demco, D. E.; Zhu, X.; Vinokur, R.; Conradi, R.; Fechete, R.; Möller, M. Water Self-diffusion Anisotropy and Electrical Conductivity of Perfluorosulfonic Acid/SiO_2 Composite Proton Exchange Membranes. *Chem. Phys. Lett.* **2012**, *554*, 143−149.
(40) Jiang, Z.; Zhao, X.; Fu, Y.; Manthiram, A. Composite Membranes Based on Sulfonated Poly(ether ether ketone) and SDBS-Adsorbed Graphene Oxide for Direct Methanol Fuel Cells. *J. Mater. Chem.* **2012**, *22*, 24862−24869.
(41) Hoarfrost, M. L.; Tyagi, M. S.; Segalman, R. A.; Reimer, J. A. Effect of Confinement on Proton Transport Mechanisms in Block Copolymer/Ionic Liquid Membranes. *Macromolecules* **2012**, *45*, 3112−3120.
(42) Tseng, C. Y.; Ye, Y. S.; Cheng, M. Y.; Kao, K. Y.; Shen, W. C.; Rick, J.; Chen, J. C.; Hwang, B. J. Sulfonated Polyimide Proton Exchange Membranes with Graphene Oxide show Improved Proton Conductivity, Methanol Crossover Impedance, and Mechanical Properties. *Adv. Energy Mater.* **2011**, *1*, 1220−1224.